PCP
PLANT & CELL PHYSIOLOGY

Challenge Integrity: The Cell-Penetrating Peptide BP100 Interferes with the Auxin–Actin Oscillator

Kai Eggenberger[1], Papia Sanyal[2], Svenja Hundt[1], Parvesh Wadhwani[2], Anne S. Ulrich[2] and Peter Nick[1,*]

[1]Botanical Institute and DFG-Center of Functional Nanostructures (CFN), Karlsruhe Institute of Technology (KIT), Kaiserstr. 12, 76133 Karlsruhe, Germany

[2]Institute of Biological Interfaces (IBG-2), and DFG-Center of Functional Nanostructures (CFN), Institute of Organic Chemistry, Karlsruhe Institute of Technology (KIT), Fritz-Haber Weg 6, D-76131 Karlsruhe, Germany

*Corresponding author: E-mail, peter.nick@kit.edu; Fax, +49-721-608-44193.

(Received March 14, 2016; Accepted September 12, 2016)

Regular Paper

Actin filaments are essential for the integrity of the cell membrane. In addition to this structural role, actin can modulate signaling by altering polar auxin flow. On the other hand, the organization of actin filaments is modulated by auxin constituting a self-referring signaling hub. Although the function of this auxin–actin oscillator is not clear, there is evidence for a functional link with stress signaling activated by the NADPH oxidase Respiratory burst oxidase Homolog (RboH). In the current work, we used the cell-penetrating peptide BP100 to induce a mild and transient perturbation of membrane integrity. We followed the response of actin to the BP100 uptake in a green fluorescent protein (GFP)-tagged actin marker line of tobacco Bright Yellow 2 (BY-2) cells by spinning disc confocal microscopy. We observed that BP100 enters in a stepwise manner and reduces the extent of actin remodeling. This actin 'freezing' can be rescued by the natural auxin IAA, and mimicked by the auxin-efflux inhibitor 1-napthylphthalamic acid (NPA). We further tested the role of the membrane-localized NADPH oxidase RboH using the specific inhibitor diphenyl iodonium (DPI), and found that DPI acts antagonistically to BP100, although DPI alone can induce a similar actin 'freezing' as well. We propose a working model, where the mild violation of membrane integrity by BP100 stimulates RboH, and the resulting elevated levels of reactive oxygen species interfere with actin dynamicity. The mitigating effect of auxin is explained by competition of auxin- and RboH-triggered signaling for superoxide anions. This self-referring auxin–actin–RboH hub might be essential for integrity sensing.

Keywords: Actin • Auxin • BP100 • Respiratory burst oxidase Homolog (RboH) • Tobacco (*Nicotiana tabacum* L.) BY-2.

Abbreviations: BDM, 2,3-butanedione monoxime; BFA, brefeldin A; BP100, KKLFKKILKYL-amide; CCP, cell-penetrating peptide; DPI, diphenyl iodonium; FABD2, actin-binding domain 2 of plant fimbrin; FITC, fluorescein isothiocyanate; GFP, green fluorescent protein; LatB, latrunculin B; NOS, nitric oxide synthase; NPA, 1-napthylphthalamic acid; PA, phosphatidic acid; PIP_2, phosphatidylinositol 4,5-bisphosphate; RboH, Respiratory burst oxidase Homolog; RFP, red fluorescent protein; TIBA, 2,3,5-tri-iodobenzoic acid.

Introduction

The dynamic self-organization of cells relies to a large extent on specific interactions between proteins mediated by astonishingly short peptide motifs. Genetic engineering has made it possible to manipulate these interactions by altering the nucleotide sequences encoding the interaction sites. As an alternative to this indirect strategy of manipulation, it should also be possible to interfere with protein–protein interactions by adding tailored peptides (for a review, see Colombo et al. 2015). However, the application of chemical engineering is limited by the fact that exogenous peptides cannot cross the membrane barrier without specific carriers. Since pathogens have to overcome membrane barriers in order to manipulate host cells, peptides that are able to cross the membrane barrier have evolved independently in several groups of organisms. For instance, the evolution of biotrophic oomycete pathogens was mainly driven by the development of versatile and often host-specific effector peptides (Jiang and Tyler 2012) These so-called cell-penetrating peptides (CPPs) which include the famous nuclear transcription activator protein (Tat) of HIV or transportan (Fanghänel et al. 2014) often harbor a high density of basic residues or exhibit an amphiphilic character (Wender et al. 2000). The possibility to exploit these CPPs as vehicles to convey functional cargoes such as RNA, DNA, drugs, peptides or even proteins into cells of interest has attracted considerable attention, although the mechanisms of membrane passage are not yet fully understood.

Due to their promising potential for medical applications, mammalian cells have clearly been the focus of this strategy. However, several reports have shown that plant protoplasts (Unnamalai et al. 2004, Chang et al. 2005, Chugh and Eudes 2007, Chugh and Eudes 2008) and even walled cells (Mizuno et al. 2009) are also competent for the uptake of CPPs. In addition to fluorescently labeled CPPs (Eggenberger et al. 2011), the rapid uptake of biomimetic peptoids could be shown for walled tobacco cells (Eggenberger et al. 2009). This uptake

Plant Cell Physiol. 58(1): 71–85 (2017) doi:10.1093/pcp/pcw161, Advance Access publication on 24 October 2016, available online at www.pcp.oxfordjournals.org

was found to be partially dependent on actin, indicating that a membrane-associated subpopulation of microfilaments might facilitate membrane passage. In fact, a fine meshwork of dynamic actin directly subtending the plasma membrane has been found to be essential for the resistance of membrane integrity against electrical (Hohenberger et al. 2011) and osmotic challenges (Liu et al. 2013). This functional subpopulation of actin complements the intensively studied transvacuolar actin cables that structure transvacuolar cytoplasmic strands (Sheahan et al. 2007) and are important for transport of organelles, such as peroxisomes (Mathur et al. 2002), chloroplasts (Kadota et al. 2009), mitochondria (Van Gestel et al. 2002) or Golgi vesicles (Boevink et al. 1998).

Since the membrane-adjacent actin seems to be relevant for membrane integrity, we wondered whether this actin subpopulation might be functionally linked to the uptake of CPPs. As an experimental model, we used the short cationic peptide BP100 (KKLFKKILKYL-amide). To follow uptake, this peptide was also used as a derivative, where a fluorescein isothiocyanate (FITC) residue was conjugated to the N-terminus. The peptide BP100 is amphiphilic and can pass the membrane in α-helical form. BP100 had been designed on the base of cecropin A (a naturally occurring peptide with antimicrobial activity found in the moth *Hyalophoracecropia*) and melittin (the membrane-permeabilizing component of bee venom), and tailored for activity against phytopathogenic bacteria such as *Pseudomonas syringae* or *Xanthomonas vesicatoria* (Ferre et al. 2006, Badosa et al. 2007, Badosa et al.2009). In our previous work (Eggenberger et al. 2011), we could show that BP100 can penetrate across the plasma membrane into living, walled tobacco cells independent of endocytosis. While uptake was found to be constrained by the presence of microtubules, it was dependent on the actin cytoskeleton. As a further step towards plant chemical engineering, BP100 was later used as vehicle to deliver the small actin-binding peptide Lifeact as functional cargo, and indeed this cargo targeted specifically to actin filaments in living tobacco Bright Yellow 2 (BY-2) cells (Eggenberger et al. 2011).

Making use of a green fluorescent protein (GFP)-tagged actin marker line in the cellular model tobacco BY-2 in combination with spinning disc confocal microscopy, we show in the current work that the uptake of BP100 occurs in a discontinuous manner, and that the membrane-adjacent cortical actin filaments respond to BP100 by reduced dynamicity, causing a rigid, frozen morphology of these filaments. The term 'actin dynamicity' which is used throughout this work is defined as an operational parameter of global actin dynamics comprising elongation and shortening of F-actin as well as lateral displacement of filaments. The unexpected 'actin-freezing' effect of BP100 can be rescued by exogenous natural auxin (IAA). In addition, the effect of BP100 upon cortical actin can be suppressed in a strongly synergistic manner, when the membrane-localized NADPH oxidase Respiratory burst oxidase Homolog (RboH) is inhibited by diphenyl iodonium (DPI). We integrate these data into a working model, where BP100 appears to interfere with the oscillatory auxin–actin circuit (for a review, see Nick 2010). This dynamic regulatory circuit might function to sense membrane integrity, as an important input for the signaling regulating programmed cell death, for instance in the context of plant defense (Chang et al. 2015).

Results

The uptake of BP100 is discontinuous and dependent on balanced actin dynamics

To investigate the response of plant cells to the cell-penetrating peptide BP100, we first determined the time course and dose dependency of uptake, making use of a fluorescent conjugate of BP100 with FITC at the N-terminus. The uptake was quantified by measuring the mean fluorescence intensity of the fluorescent reporter, corrected for background intensity. The cells were investigated at day 3 after subcultivation, a time point where proliferation activity has already ceased (Maisch and Nick 2007), such that only interphase cells were tested. To obtain reliable results, the signal to noise ratio was adjusted by raising the concentration of the fluorescent BP100 to 4 μM. This time course was clearly discontinuous (**Fig. 1A**): After a rapid onset, uptake stopped at around 30 min, but resumed at 60 min and continued till 90 min, halted again for about 30 min and then restarted at 120 min, up to150 min when the uptake was saturated. Each of these three cycles of uptake and pause increased the total intracellular abundance of the fluorescent reporter. However, during each of these cycles, the increase in signal intensity became smaller—thus, the third step (from 120 min) yielded only half the increase seen during the first step. Since the time interval of the experiment (2.5 h) is too small to generate any measurable increase of cell number or cell volume, the progressive slowdown of uptake cannot be accounted for by a dilution of the peptide, but must be an innate property of uptake. A dose–response curve measured at 120 min (**Fig. 1B**) showed a significant uptake already for 0.5 μM BP100, and saturation between 5 and 10 μM. Half-maximal uptake was observed for 3.5 μM. In the next step, we examined to what extent this uptake was dependent on actin, using both pharmacological and genetical manipulation. When actin filaments were eliminated by latrunculin B (LatB; **Fig. 1C**), this caused a small but significant reduction of uptake (by about 30%). The same effect was observed when the dynamics of actin filaments were suppressed by treatment with phalloidin (Pha; **Fig. 1C**). Again, uptake was decreased by about 30%. In contrast, in cells overexpressing tobacco WLIM1, a protein stabilizing actin filaments, uptake was almost doubled, whereas in cells overexpressing the actin-bundling protein tobacco villin (VLN1; **Fig. 1C**), uptake was reduced by about 60%. When the actin-binding domain 2 of plant fimbrin (FABD2)—used as a state-of-the art marker for plant actin (but producing a mild stabilization of actin filaments)—was overexpressed, this stimulated uptake almost 3-fold. In contrast, the non-plant actin-binding protein mouse talin, and the yeast-derived peptide Lifeact [in fusion with a photoswitchable red fluorescent protein (RFP), LApsRFP] did not produce any significant changes in uptake. To test whether the stimulation of uptake by WLIM1 and FABD2, and the inhibition by villin or phalloidin might be correlated with a different degree of stabilization

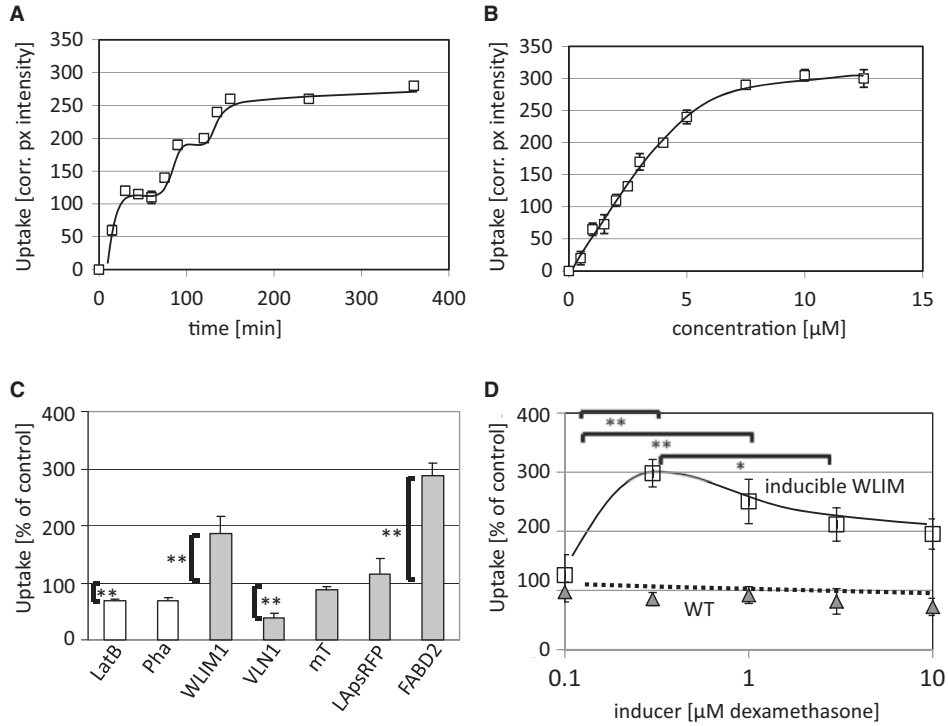

Fig. 1 The uptake of BP100 depends on actin. (A) Time course of uptake of 4 µM FITC-conjugated BP100 measured by mean fluorescence intensity, corrected for background intensity. (B) Dose–response relationship of uptake measured after 2 h. (C) Actin dependency of uptake. Uptake of 2 µM FITC-conjugated BP100 measured at 2 h either after pharmacological treatment (white bars) or in genetically engineered strains of BY-2 (gray bars), relative to the uptake measured in non-transformed untreated controls. LatB (500 nM), phalloidin (Pha, 1 µM), the WLIM1 line expressing tobacco WLIM1 in fusion with GFP under control of the 35S promotor, the VLN1 line expressing tobacco Villin 1 in fusion with GFP under control of the 35S promotor, the mT line expressing mouse talin in fusion with GFP under control of the 35S promotor, the LApsRFP line expressing Lifeact in fusion with photoswitchable RFP under control of the 35S promoter, and the FABD2 line expressing the actin-binding domain 2 of Arabidopsis fimbrin under control of the 35S promote. (D) Dexamethasone-inducible stimulation of uptake (plotted as percentage uptake in the untreated WLIM line) for inducible expression of the WLIM-domain (open squares) compared with treatment of the non-transformed wild type (gray triangles). Data points give the mean and SE from around 150–200 individual cells collected from three independent experimental series. Brackets indicate significant differences, with $^{*}P < 0.05$ and $^{**}P < 0.01$.

conferred by these molecules, we used a cell line in which the actin-stabilizing LIM domain was expressed under control of a dexamethasone-inducible promoter (**Fig. 1D**). We observed that a low concentration of the inducer (0.3 µM) produced a strong (almost 3-fold) stimulation of uptake, whereas this stimulation decreased progressively when the concentration of the inducer was raised. A non-transformed wild type, treated in parallel as a negative control, did not show any stimulation of uptake in response to dexamethasone (**Fig. 1D**; gray triangles). This finding indicates that the degree of stimulation depends on the extent of actin stabilization. Taken together, it appears that BP100 is taken up in a stepwise manner depending on actin dynamics.

The uptake of BP100 depends on apical dominance within the cell file

Suspension cells of tobacco divide axially, generating a pluricellular file that—with respect to several features such as synchronization of cell division by a directional flux of auxin—behaves like a very simple organism (for a review, see Opatrný et al. 2014). Here, the apical cell acts as the organizer and also differs with regard to a gradient of the actin nucleation factor Arp3 (Maisch et al. 2009). We therefore asked whether the uptake of BP100 would differ depending on the position of the cell along the cell file. In order to ensure that potential differences reflect steady-state levels and not just kinetic differences of accumulation, we scored the result 2 h after addition of the fluorescent BP100 conjugate. The concentration of the fluorescent BP100 had to be selected sufficiently high to ensure a robust ratio of signal to noise. Since we recorded a single time point, where uptake was already saturated, rather than a short-term time course of uptake, a concentration of 2 µM was found to be sufficient. Indeed, the uptake of fluorescently labeled BP100 into the apical cells was clearly elevated compared with the downstream cells in the file (**Fig. 2A**). This difference (termed in the following as apical dominance Δ) was quantified by integrating the fluorescence intensity in the apical vs. the subapical cell, and relating this difference to the total intensity integrated over both cells (**Fig. 2C**). Apical dominance was pronounced under control conditions, with more than two-thirds of uptake in the first two cells being partitioned to the apical cell. When followed over time (**Fig. 2D**), apical dominance was manifest from the beginning. However, apical

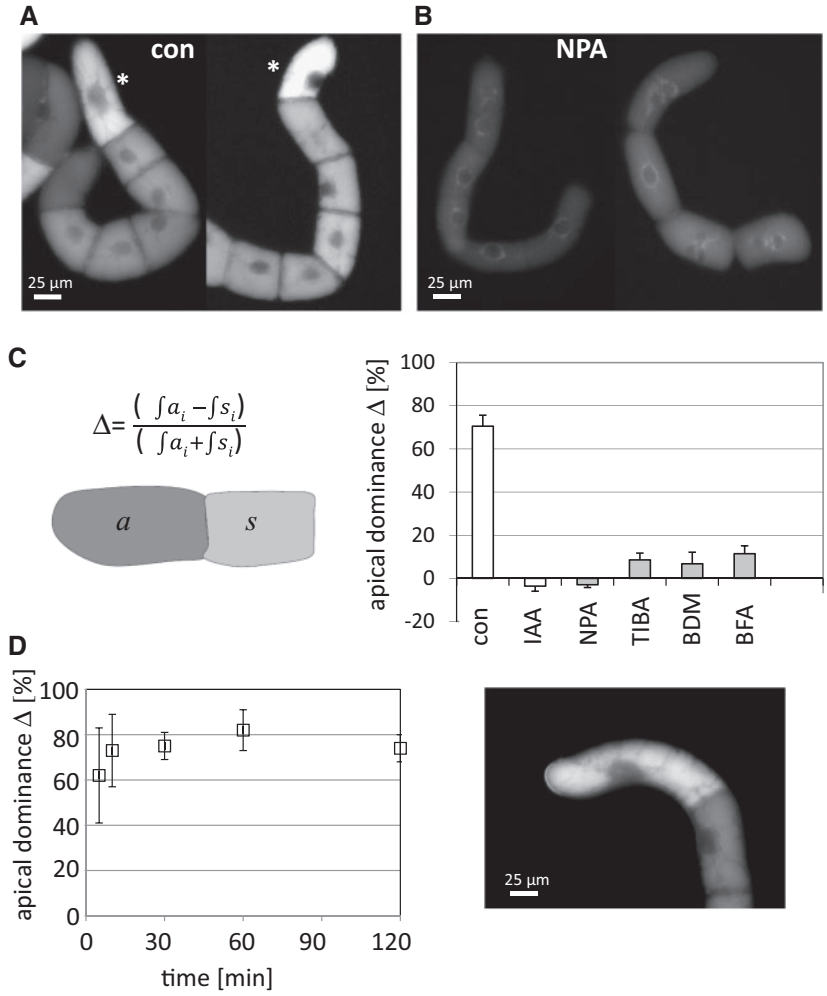

Fig. 2 Apical dominance of BP100 uptake. (A) Representative images of control cells (con) incubated with 2 µM FITC-conjugated BP100 for 2 h. Note the preferential uptake into the apical cells (asterisks) over the other cells of a file. (B) Representative images of cells pre-incubated with NPA (50 µM) before incubation with 2 µM FITC-conjugated BP100. (C) Quantification of apical dominance Δ, defined as the ratio between integrated pixel density in the apical cell (a_i) over the subapical cell (s_i) over the total integrated pixel density ($a_i + s_i$), for controls or following pre-treatment for 4 h with the natural auxin IAA (10 µM), the auxin transport inhibitor NPA (50 µM), the auxin transport inhibitor TIBA (20 µM), the myosin inhibitor BDM (30 µM) and the secretion inhibitor BFA (10 p.p.m.). (D) Temporal development of apical dominance Δ in control cells incubated with 2 µM BP100–FITC. A representative cell file recorded 10 min after addition of the conjugated peptide.

dominance was very sensitive to pharmacological manipulation targeted to auxin: exogenous IAA, as well as inhibition of polar auxin transport by 1-*N*-naphthylphthalamic acid (NPA) or 2,3,5-triiodobenzoic acid (TIBA), could completely eliminate the gradient of uptake into the apical cell. As a consequence, overall uptake into the cell file was strongly reduced after treatment with these inhibitors (shown exemplarily for NPA in **Fig. 2B**). The same holds true for the myosin inhibitor 2,3-butanedione monoxime (BDM) and brefeldin A (BFA), an inhibitor of vesicle traffic that perturbs the localization of membrane proteins including the PIN proteins as putative auxin-efflux transporters (**Fig. 2C**). These inhibitors eliminate apical dominance by reducing the preferential uptake of BP100 into the apical cell. The elimination of apical dominance is even accentuated by the fact that the uptake into the non-apical cells was also decreased. As a consequence, the signal in the apical cell becomes as low as in the downstream cells of the file (**Fig. 2B**).

BP100 causes rapid and reversible freezing of cortical actin filaments

Since the uptake of BP100 was found to depend on actin dynamics (**Fig. 1**), and since dynamic actin filaments subtend the plasma membrane, we investigated the response to BP100 by recording time-lapse series for this dynamic actin population and quantifying the dynamics of actin remodeling (Nick et al. 2009). This remodeling is a complex phenomenon comprising rapid processes such as elongation of filaments, shortening of filaments or lateral displacements (exemplarily shown in **Fig. 3E**), accompanied by slower processes such as bundling. As an operational parameter integrating over these individual processes, we introduced 'actin dynamicity'. This actin dynamicity is to be distinguished from actin dynamics in the conventional sense of assembly and disassembly, and was determined as the differential of F-actin in subsequent frames of a time-lapse series. To follow actin dynamicity, we used an FABD2–

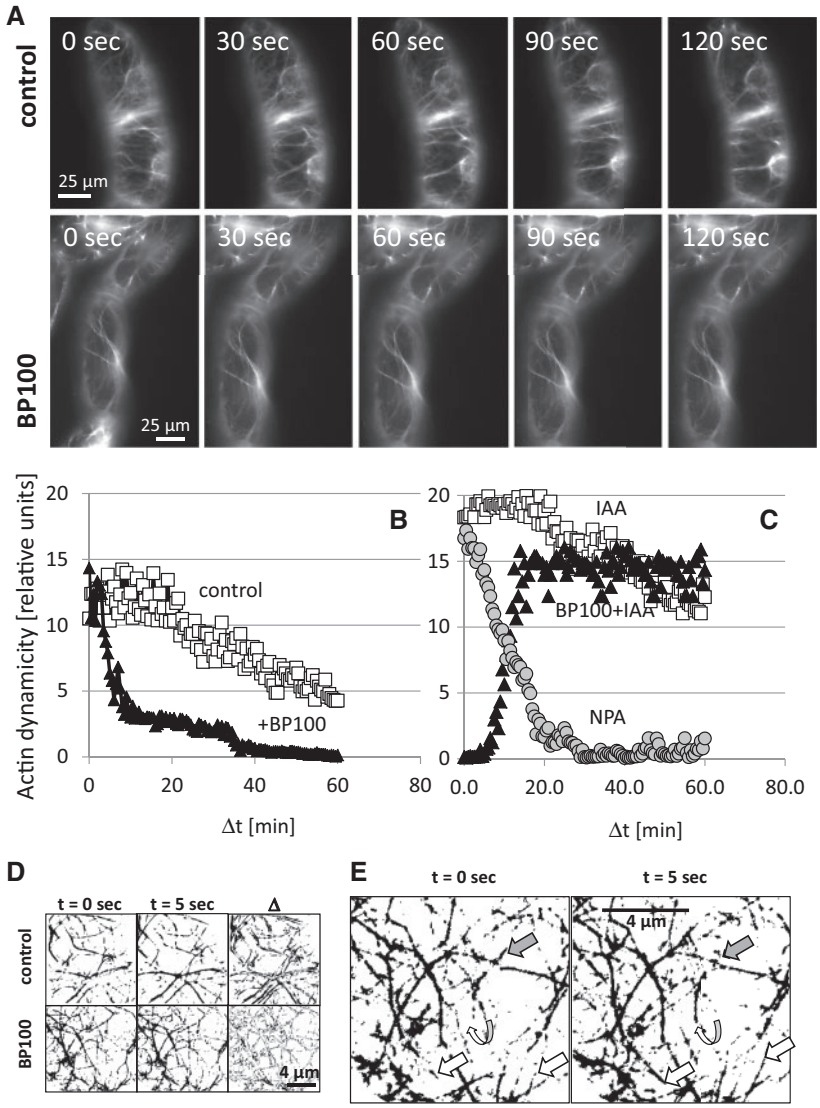

Fig. 3 BP100 causes rapid freezing of actin filaments as visualized in the FABD2–GFP marker line. (A) Representative sequence of frames from a time-lapse series of a control cell (upper row) and after treatment with 1 µM BP100 (lower row), time interval 30 s. (B) Changes of actin dynamicity (for details, see the Materials and Methods) over time in a control cell (open squares) as compared with a cell treated with 1 µM BP100 (filled squares). BP100 was mixed with the cells before mounting to ensure rapid access. Due to the time required for mounting and adjustment of microscopy, observation started 3 min after addition of BP100. (C) Restoration of actin dynamicity by 2 µM IAA added 2 h after 1 µM BP100 (filled triangles), and loss of actin dynamicity in response to 50 µM NPA (gray circles) as compared with a control cell without pre-treatment (open squares). (D) Quantification of actin dynamicity. Subsequent frames of a time series were inverted and converted into binary images. The absolute difference between these frames (Δ) was integrated over the area of the frame. The ratio of this value and the area of the region of interest was used as a measure for the dynamic change of actin organization. (E) Processes contributing to actin dynamicity from two subsequent frames of a time series collected from a control sample. Actin elongation (white arrows), actin shrinkage and/or severing (gray arrows) and actin swaying (bent arrow) as events of rapid actin change (bundling is slower and can be measured only over longer time spans).

GFP fusion construct with the actin-binding domain 2 of plant fimbrin, a state-of-the-art marker with only mild effects on actin dynamics (for a discussion of this aspect, refer to Guan et al. 2014). In fact, cortical actin filaments revealed extensive remodeling when projections of confocal *z*-stacks collected at subsequent time points were compared. Even when the time interval was reduced to 30 s, which was the minimal time to record a *z*-stack through the cell, extensive remodeling could be seen between subsequent frames (**Fig. 3A**; **Supplementary Movies S1, S2**). This high dynamicity persisted over the first 20 min of observation (**Fig. 3B**), but later decreased slowly and dropped to around half the initial value. In contrast to the high dynamicity in the control, cells treated with 1 µM BP100 rapidly lost actin dynamicity (**Fig. 3A**; **Supplementary Movie S3**). To avoid irreversible cellular damage, a low concentration of 1 µM was chosen for the peptide in this and all subsequent experiments. Nevertheless, the drop in actin dynamicity was clearly of a different quality when compared with the slow decrease observed in the control from 20 min after onset of imaging (**Fig. 3B**). The BP100-induced loss of actin dynamicity was

very rapid—already in <10 min the dynamicity had dropped to around 25% of the initial value, and continued to decrease further such that after 40 min the actin filaments appeared to be completely frozen and immobile. To test whether this loss of 'actin dynamicity' was irreversible, we conducted a rescue experiment with the natural auxin IAA, which can restore a normal actin organization in cells, where actin is bundled due to overexpression of the actin-binding protein mouse talin (Maisch and Nick 2007, Kusaka et al. 2009). Indeed, it was possible to re-initiate actin dynamicity in cells in which the treatment with BP100 had led to a complete immobilization of the actin filaments (**Fig. 3C**; **Supplementary Movie S4**). This recovery was rapid and complete—within 15 min after addition of 2 μM IAA, the dynamicity had returned to the values observed in the control. This experiment also showed that the concentration of 1 μM BP100 was low enough to avoid irreversible damage over the time span of this type of experiments. To gain insight into some of the elementary processes underlying actin dynamicity, we quantified elongation and shortening rates in randomly selected sets of individual actin bundles, and also determined apparent bundle thickness for the key conditions of the experiments described above (**Supplementary Table S1**). Under control conditions, the elongation rate slightly exceeded shortening. The 'frozen' configuration of actin produced by BP100 (1 μM over 2 h) was accompanied by a strong decrease of both elongation and shortening, and a >2-fold increase of apparent bundle thickness. Treatment with IAA (2 μM over 30 min) more than doubled the elongation rate and caused a slight (by around one-third) decrease of apparent bundle thickness. When IAA was administered to the 'frozen' filaments produced by BP100 (1 μM over 2 h), apparent bundle thickness returned to the value found in control cells, and elongation and shortening rates were also rescued. To test whether depletion of endogenous IAA can phenocopy the effect of BP100, the cells were treated by 50 μM NPA, an inhibitor of auxin efflux carriers. Within a few minutes after addition of this compound, dynamicity decreased strongly (**Fig. 3C**). In a control experiment, the long-term response of dynamicity to BP100 was assessed in a population of cells incubated in batch under conditions of a suspension culture (i.e. while rotating on a shaker) to avoid artificial loss of dynamicity by prolonged exposure on a microscope slide. This experiment showed rhythmic changes of dynamicity (**Supplementary Fig. S1**), where dynamicity partially recovered from 40 min, when it was low, to a higher value at 80 min, and then decreased again to a second low at 120 min, followed by a weaker recovery at 160 min.

Overexpression of actin marker FABD2–GFP accentuates negative impact of BP100

Since the dynamicity of actin is required for auxin transport (Maisch and Nick 2007, Nick et al. 2009), the reduced actin dynamicity caused by BP100 is expected to impair auxin-dependent processes, such as cell division. We therefore recorded dose–response curves for viability and mitotic index 24 h after addition of BP100 in the non-transformed BY-2 wild type and compared this with the FABD2 overexpressor line. In the non-transformed wild-type cells, concentrations of BP100 exceeding 1 μM significantly increased long-term mortality (**Fig. 4A**). This increase requires some time to develop, and becomes detectable from 6 h after addition of BP100 (Gao et al. 2016). When the concentration was raised to 10 μM, all cells died within 24 h. The half-maximal effect was reached for 5 μM BP100. Cell proliferation is blocked at much lower concentrations compared with viability (**Fig. 4B**). Here, for the non-transformed wild type, concentrations of BP100 exceeding 0.1 μM reduced the mitotic index significantly, i.e. at 1 μM, mitotic activity has dropped to less than half of the control value. This means that proliferation is inhibited at concentrations of BP100 that are around one order of magnitude lower than those causing cell death. If this negative impact of BP100 on cellular physiology is linked with actin, overexpression of the actin marker FABD2, which causes a mild stabilization of actin filaments, would be expected to accentuate the effect of BP100. In fact, the dose–response curve of mortality shows a slight shift (**Fig. 4A**), with saturation already reached at 8 μM (compared with 10 μM in the non-transformed control). However, this shift was below the threshold for statistical significance if $P = 0.05$ was considered. However, for cell proliferation (**Fig. 4B**), a clear and pronounced difference was observed (**Fig. 4B**). Here, the mitotic index became already significantly inhibited from 50 nM BP100 in the FABD2 overexpressor. Compared with the non-transformed wild type, the transgenic line was more sensitive by around one order of magnitude. Thus, overexpression of the actin-stabilizing marker FABD2 renders the cells more sensitive to the negative effect of BP100 upon mitotic activity.

Diphenylene iodonium and BP100 act antagonistically on actin freezing

We had found that the natural auxin IAA can rescue actin dynamicity after BP100 treatment (**Fig. 3C**; **Supplementary Movie S4**). In our previous work (Chang et al. 2015), we had shown that the effect of auxin on actin depends on the activity of the membrane-associated NADPH oxidase RboH (Chang et al. 2015). The superoxide anions generated by this enzyme are required for auxin signaling and are thus not able to induce actin bundling. By using DPI, a specific inhibitor of the NADPH oxidase RboH, the formation of superoxide anions should be suppressed, and this is expected to mimic the effect of auxin upon actin bundling. When DPI was administered alone, this did not cause actin freezing in most cells, even for long treatment times up to 90 min (**Fig. 5A**; **Supplementary Movie S6**). However, in a significant fraction of cell, the actin-binding domain of plant fimbrin was low (for details see below). In the next experiment, we tested whether DPI could phenocopy auxin with respect to the rescue of actin dynamicity. In this experiment, cells were first treated by BP100 for 1 h, such that actin dynamicity was completely abolished, and subsequently these cells were treated with DPI. This treatment could indeed restore actin dynamicity in some cells (**Fig. 5A**; **Supplementary Movie S7**). However, other cells were not responsive—the difference was quanitative: either a cell restored actin dynamicity

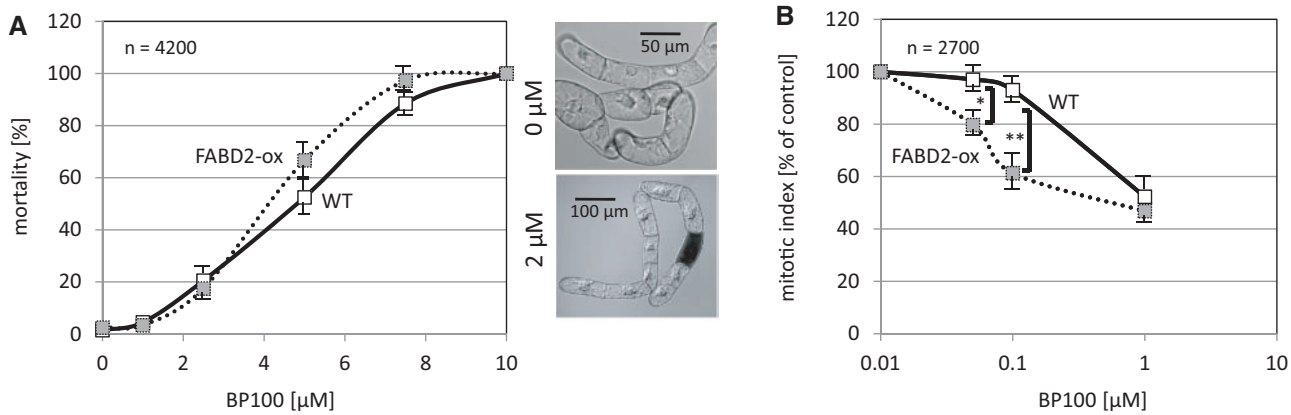

Fig. 4 Cellular responses to BP100 are more elevated in an FABD2 overexpressor line. (A) Dose–response curve for mortality 24 h after treatment. Two representative images after staining with Evan's Blue are shown. (B) The mitotic index scored in the maximum of proliferation activity (days 2–3) relative to the untreated control. Data represent mean values and SEs of three independent experimental series. Brackets indicate significant differences, with $^{*}P < 0.05$ and $^{**}P < 0.01$.

to a normal level, or it maintained completely immobile actin filaments. Even neighboring cells of one file could differ in this response (**Supplementary Movie S7**). Interestingly, a similar all-or-none-type heterogeneity could be observed when early stages (15–20 min) of the response to BP100 were examined (**Supplementary Movie S5**): some cells still maintained a high level of actin dynamicity, whereas neighboring cells already displayed virtually complete actin freezing. With prolonged incubation (60 min), this heterogeneity vanished, because the fraction of cells with persistent actin dynamicity'decreased rapidly, i.e. all cells displayed complete 'freezing' of actin. To account for this discontinuous response of actin dynamicity over the cell population, we scored frequency distributions of cells over five different levels of actin dynamicity (**Fig. 5D**) in control cells, in cells treated for 90 min with BP100 (1 µM), in cells treated for 90 min with DPI (200 nM) and in cells that had been treated first for 60 min with BP100 and subsequently with DPI for an additional 30 min. For the control, the vast majority of cells clustered to the upper two levels of actin dynamicity. In contrast, treatment with BP100 shifted the entire distribution into the two lowest levels. Upon treatment with DPI alone, the majority of cells maintained high levels of dynamicity, but in contrast to the control there was a significant proportion with frozen actin as well. The effect of DPI on cells that had been pre-treated with BP100 was very clear: here the two highest dynamicity levels clearly prevailed; hence, this treatment almost completely restored the situation in the control. Interestingly, the fraction with immobile actin found in the experiment where DPI had been applied alone was significantly reduced after preceding incubation with BP100. Thus, DPI can rescue BP100-induced actin freezing. However, it is also clear that actin dynamicity is not manifest as a continuous effect, but rather in a highly discrete manner over each individual cell. Individual cells either are in a state of high actin dynamicity, or actin dynamicity is almost completely shut off. Both states can co-exist even in neighboring cells of a file. Especially during early phases of a response (**Supplementary Movie S5**), or in a situation where the effect on actin dynamicity is not saturated (DPI alone in **Fig. 5D**; **Supplementary Movie S7**), this cellular heterogeneity becomes manifest.

Discussion

In the current work, we have addressed cellular mechanisms modulating the import of the short cationic cell-penetrating peptide BP100, which is able to permeate membranes as an amphiphilic α-helix. We see a discontinuous uptake of BP100 proceeding in cycles of around 20–30 min duration. Each cycle comprises a phase of rapid uptake, followed by a phase in which transport is mostly halted. Moderate stabilization of actin promotes import, whereas elimination of actin or suppression of its 'dynamicity' (an operationally defined parameter describing the global extent of remodeling) inhibit uptake. BP100 enters preferentially into the terminal cell of the pluricellular tobacco cell files, and this asymmetry is dependent on auxin transport. The preference for the terminal cells can be eliminated either by inhibitors of polar auxin transport, or by over-riding the auxin gradient along the file by addition of the natural auxin IAA. We therefore addressed the effect of IAA on the response of actin filaments to BP100 and could show that IAA could rescue actin dynamicity. It should be kept in mind that BY-2 cells (like other tobacco suspension lines) are cultivated in the presence of exogenous 2,4-D. However, the effect on actin is only observed for auxin species capable of polar transport (Maisch and Nick 2007, Nick et al. 2009). The fact that 'actin dynamicity' is also present under control conditions is explained by the activation of endogenous IAA in response to the 2,4-D present in the medium (Qiao et al. 2010). Conversely, block of polar auxin transport by NPA can mimick the effect of BP100 with respect to actin 'freezing'. We also demonstrate that the negative impact of BP100 on viability and mitotic activity is accentuated in a cell line overexpressing FABD2, conferring a mild stabilization of actin. In the search for a mechanism that would transduce the impaired membrane integrity caused by BP100 to the morphology of actin, we investigated the role of the

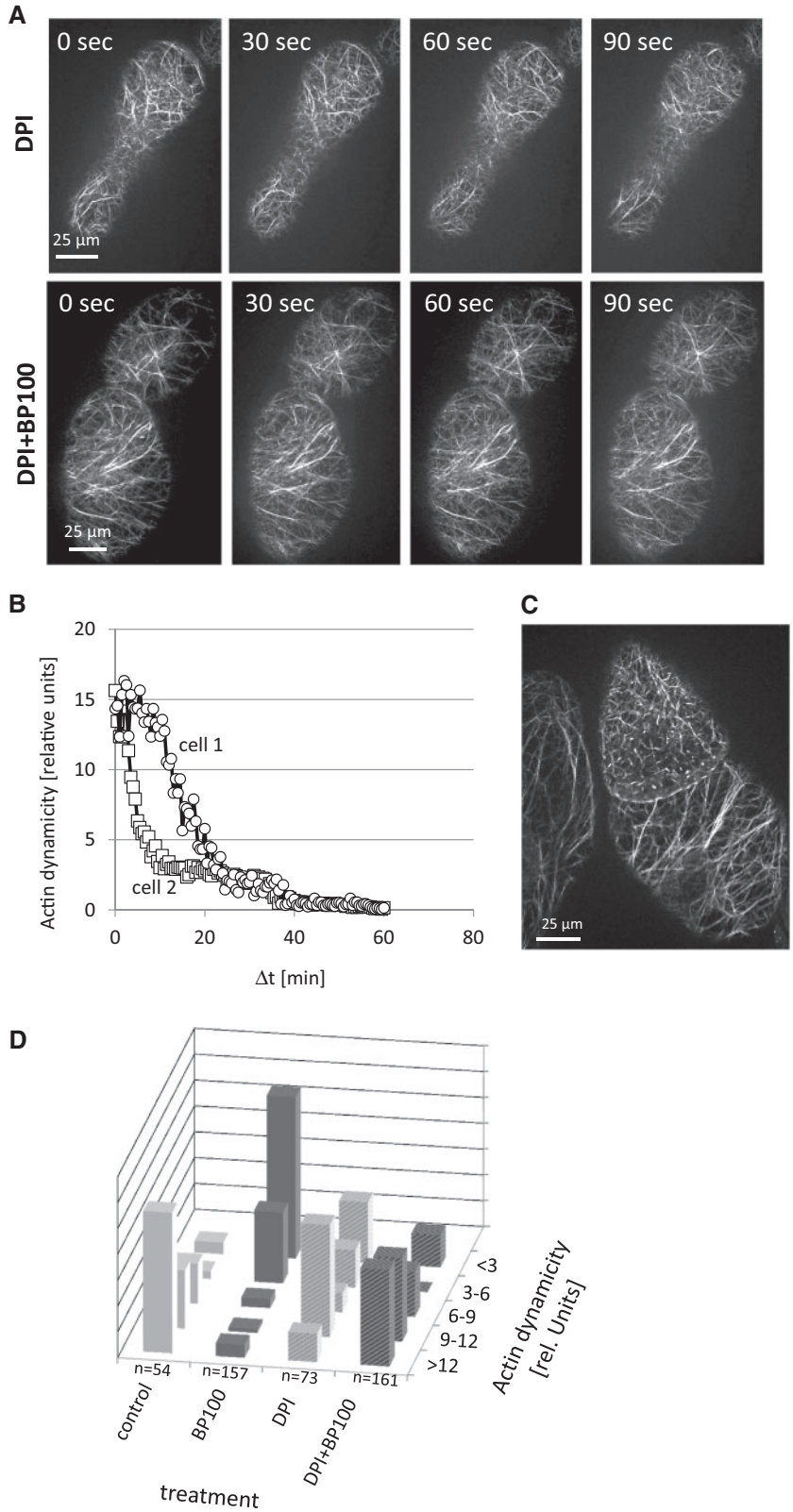

Fig. 5 Restoration of actin dynamicity by DPI in the FABD2–GFP cell line. (A) Representative sequence of frames from a time-lapse series of a cell that has been treated for 90 min with 200 nM DPI (upper row), and a cell that has been treated with 1 µM BP100 for 1 h and then with 200 nM DPI for 30 min (lower row), time interval 30 s. (B) Cellular heterogeneity in the response to BP100. Actin dynamicity in two neighboring cells of a file is shown over time after addition of 1 µM BP100. (C) Disruption of actin filaments observed in the terminal cells of a file after treatment with 1 µM BP100 for 30 min. (D) Frequency distribution over actin dynamicity for control cells, for cells that had been treated with 1 µM BP100 for 90 min, for cells that had been treated with 200 nM DPI for 30 min and for cells that had been first treated with 1 µM BP100 for 1 h and subsequently with 200 nM DPI for an additional 30 min.

membrane-localized NADPH oxidase RbohH in generating apoplastic superoxide anions. We show that inhibition of RbohH by the specific inhibitor DPI can rescue the 'actin freezing' caused by BP100, and that the response of individual cells is discontinuous with a phase transition between a normal actin dynamicity and a state in which actin filaments undergo 'freezing'.

BP100 and actin—a bidirectional relationship

The uptake of BP100 is clearly dependent on dynamic actin, because both the elimination of actin by LatB, as well as the suppression of actin dynamicity by phalloidin significantly reduced the uptake of BP100 (**Fig. 1C**). In contrast, a mild stabilization of actin by FABD2 (Zaban et al. 2013) or a stimulation of actin remodeling by the actin-binding protein WLIM (Thomas et al. 2006) were able to enhance uptake. On the other hand, the heavy bundling induced by plant villin or treatment with phalloidin reduced uptake substantially. Apparently, actin filaments not only need to be present, but they also have to be dynamic to a certain extent. To pinpoint this further, we tested uptake in a transgenic cell line, where the actin-bundling LIM domain can be induced by dexamethasone (Thomas et al. 2006), by recording the response of BP100 uptake as a function of the concentration of this inducer (**Fig. 1D**). This dose–response curve exhibited a clear maximum for low concentrations of dexamethasone, i.e. low abundance of the LIM domain, whereas the stimulation vanished, when the concentration exceeded 0.3 μM, such that the elevated abundance of the LIM domain would reduce actin dynamicity. A negative control with the non-transformed wild type did not show any stimulation of uptake in response to dexamethasone, demonstrating that the effect was caused by the expression of the LIM domain, and not by a non-specific effect of the inducer. We therefore think that the slight stabilization conferred by FABD2 is promotive, whereas the more heavy bundling conferred by mouse talin is beyond the peak (superoptimal), although not as strongly as phalloidin treatment or villin overexpression. A similar conclusion on the role of stability can be drawn when the cellular responses to different concentrations of BP100 are compared between a non-transformed wild type and a transgenic line overexpressing FABD2 (**Fig. 4**). The transgenic line, where actin is mildly stabilized compared with the wild type, is more sensitive, as manifest by a slightly but significantly increased mortality at higher concentrations of BP100. The effect becomes more evident when mitotic activity is considered. Here, the transgenic line responds to BP100 by a strong decrease of the mitotic index at concentrations that are around 10-fold lower than those needed in the wild type to produce a comparable inhibition. The dose–response curves are thus shifted by around one order of magnitude, which correlates actin stability with the response to BP100.

The role of actin for uptake is also, albeit indirectly, supported by the observation of preferential uptake into the apical cell (**Fig. 2**). This apical dominance was present from the beginning, as revealed by time course experiments (**Fig. 2D**), and did not emerge from a transitional state, where the peptide was taken up evenly and only later a gradient developed by intracellular partitioning. The apical dominance was dependent on the gradient of IAA along the file, and could be eliminated either by over-running the gradient by exogenous IAA, by inhibiting auxin efflux through phytotropins or by interfering with the proper localization of membrane transporters using BFA. As a specific cellular feature, apical cells are endowed with a significantly higher density of actin nucleation sites as compared with the subapical cells, as visualized by the nucleation marker Arp3 (Maisch et al. 2009). Thus, it appears that the apical cell, which is endowed with a gradient of Arp3 and also acts as organizer of the file, takes up BP100 much more efficiently than the downstream cells of the file. By interference with auxin gradients (either by supply of exogenous auxin or by interfering with the polarity of auxin flux), this dominance of the apical cell can be eliminated. Further evidence for the role of actin dynamicity for uptake comes from a batch experiment, where actin dynamicity was followed over a longer time span in the presence of BP100 (**Supplementary Fig. S1**). Here, rhythmic changes were observed with partial recovery of dynamicity at 80 and 160 min, which were time points at which uptake rates were high as well (**Fig. 1A**), whereas dynamicity was low at 40 and 120 min, when uptake also experienced a transient halt.

However, the observed dependence of BP100 uptake and actin dynamics co-exists with a retrograde relationship: actin dynamicity is clearly down-regulated by BP100 (**Fig. 3**; **Supplementary Movies S1–S3**). This response is rapid and complete in $<$15 min. The 'frozen' situation is linked with a strong decrease of both elongation and shortening, and an increase of apparent bundle thickness (**Supplementary Table S1**). The remodeling of submembraneous actin is a complex process that involves severing of longer filaments, probably by actin-depolymerization factors and cofilins, nucleation of new filaments (Smertenko et al. 2010) as well as interaction with microtubules, presumably via specific formins (Deeks et al. 2010). In addition, cortical filaments are physically linked with the plant cell membrane as shown by TIRF (total internal reflection fluorescence) microscopy (Hohenberger et al. 2011), for instance via actin-depolymerization factor 2 which can modulate actin dynamics through sensing the abundance of membrane-anchored phosphatidylinositol 4,5-bisphosphate (PIP_2), dependent on signaling events in the membrane (Durst et al. 2013, Chang and Nick 2015). Thus, although the molecular mechanisms underlying the interaction between BP100 and the dynamic actin filaments subtending the plasma membrane still need to be identified, there exist several molecular candidates that might qualify for this task. Since actin elongation resumes when the 'frozen' state that had been induced by BP100 is rescued by IAA (**Supplementary Table S1**), factors that regulate elongation of filaments are of special interest.

BP100, the auxin–actin oscillator, and cellular phase transitions

The reduction of actin dynamicity induced by BP100 can be rescued by addition of exogenous auxin (**Fig. 3**; **Supplementary Movie S4**), indicating that both auxin and BP100 converge antagonistically upon the same actin-interacting proteins. This is

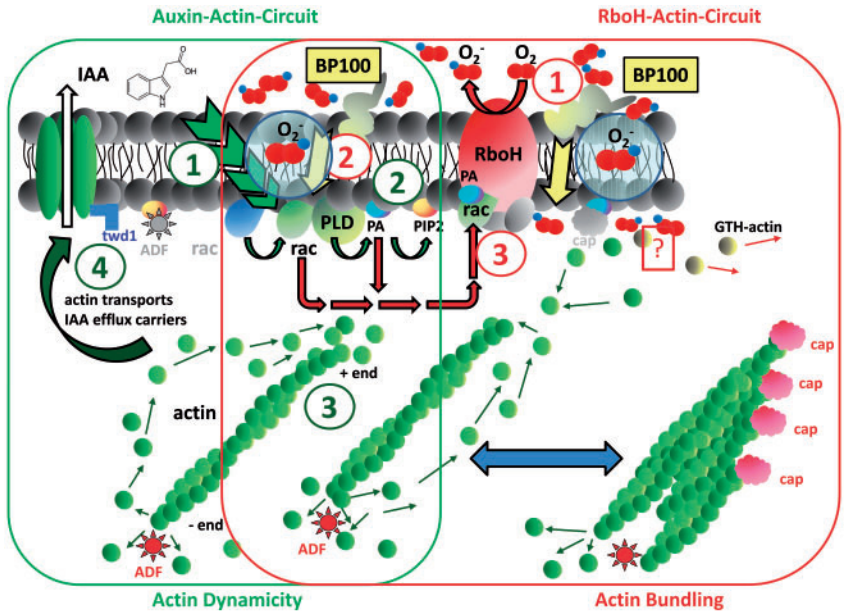

Fig. 6 Working model for the interaction of BP100 with the auxin–actin (green) and the RboH–actin (red) circuits. The auxin–actin circuit initiates by the docking of auxin (IAA) to a receptor at the plasma membrane, which triggers transmembrane signaling using superoxide anions (green ①), resulting in the activation of the small G-protein Rac that will transduce the signal into an activation of phospholipase D generating phosphatidic acid (PA), which can be further converted into PIP_2 (green ②). PA can sequester actin-capping proteins (cap) to the membrane, facilitating the elongation of actin filaments, whereas PIP_2 can bind actin-depolymerization factor (ADF), which will reduce disassembly at the minus ends of actin filaments (green ③). As a result, actin filaments are dynamically elongating, which is supporting localization of auxin-efflux carriers (possibly in a complex with twisted dwarf 1) at the plasma membrane (green ④) such that the concentration of auxin in the apoplast will increase. The RboH–actin circuit initiates by the partial reduction of apoplastic oxygen into superoxide anions (red ①) by the NADPH oxidase Respiratory burst oxidase Homolog (RboH). This reaction is constitutively active to a certain extent and is necessary to sustain growth, for instance by providing superoxide anions necessary to support auxin signaling (green ①). However, in contact with BP100, the passage of superoxide anions becomes elevated—either because the activity of RboH is induced or because the permeability of the membrane to superoxide anions is temporarily increased as a consequence of BP100 membrane passage. The membrane passage of superoxide anions that are not recruited for auxin signaling will stimulate binding of Rac to PA, and this complex is then committed for the activation of RboH (green ③). This will reduce the abundance of PA available for the sequestration of capping proteins that are therefore released and block actin elongation. Moreover, the conversion of PA into PIP_2 will be reduced, such that ADF is also released from the membrane, stimulating decay of dynamic actin filaments. The excess G-actin will then result in actin bundling. In parallel, penetrating superoxide anions will stimulate glutathionylation of G-actin, which then will not be able to reintegrate into filaments (red ?).

also supported by the finding that NPA, an inhibitor of auxin efflux, can phenocopy the effect of BP100 on actin dynamicity, probably by causing a depletion of intracellular auxin (**Fig. 3C**). The modulation of actin remodeling by auxin has been shown previously for different plant responses, such as division synchrony over the pluricellular cell files of tobacco (Maisch and Nick 2007), or the regulation of tropistic growth responses in rice (Nick et al. 2009). Since, on the other hand, auxin transport depends on actin (for a recent review, see Zhu and Geisler 2015), this will establish a regulatory circuit.

In the following, we propose details of this regulatory circuit and its interaction with BP100. This working model is based upon a model derived from the interaction between auxin and defense (Chang et al. 2015). As a working model, it has two functions: to explain the data so far and to stimulate future experiments. It therefore contains molecular elements that have not yet been validated experimentally, but are testable in future work. This model predicts that actin filaments as well as auxin efflux change their dynamics in an oscillatory manner (reviewed in Nick 2010) with a period of around 20–30 min (**Fig. 6**, green numbers). For division synchrony, the role of different actin-binding proteins for the auxin response of actin has been investigated in more detail (Durst et al. 2013). This search identified actin-depolymerization factor 2 that can—dependent on the auxin status—shuttle between actin and the cytoplasmic face of the cell membrane: In the presence of auxin, phosphatidic acid (PA) and its derivative PIP_2 will accumulate at the membrane. Both molecules can then sequester different actin-binding proteins. PIP_2 binds actin-polymerization factor 2 (Van Troys et al. 2008, Durst et al. 2013), which will result in reduced treadmilling of actin at the minus end and, consequently, an increased stability of actin filaments. Consistent with this hypothesis, the elongation rate of F-actin is promoted by exogenous IAA (**Supplementary Table S1**). On the other hand, PA will sequester actin-capping proteins to the membrane (Li et al. 2012), such that the elongation of filaments is promoted. In the absence of auxin, PA is recruited for other targets, such that PIP_2 will be depleted, leading to a release of actin-depolymerization factor 2 from the membrane (Durst et al. 2013). This will now stimulate actin depolymerization at the

minus-end (Ressad et al. 1998). At the same time, since PA is diverted towards other processes, actin-capping proteins will be released as well, which will limit the elongation of actin filaments. Under these conditions, severing proteins (Su et al. 2007) and additional actin nucleation triggered by the released excess G-actin will result in the formation of thicker actin cables (Moldovan et al. 1998). This mechanism does not exclude the existence of parallel pathways, for instance a complex between the actin-binding protein twisted-dwarf 1 (twd1) and the auxin efflux system (reviewed in Zhu and Geisler 2015). Mediated by such pathways, actin filaments can therefore switch between a state in which they actively elongate and remain thin, and a state in which they halt elongation and undergo bundling. Since the uptake of BP100 depends on the dynamicity of cortical actin, whereas on the other hand actin dynamicity is modulated by BP100, a self-referring regulatory circuit is expected to be established, which should oscillate with a period of around 30 min (the time required first to complete and subsequently to release bundling, **Fig. 3C**). This periodicity might account for the discontinuous uptake of BP100 (**Fig. 1A**), which oscillates with a similar period: the initial rapid uptake of BP100 will cause excessive bundling of actin, which in turn will inhibit further uptake. Subsequent recovery of actin dynamicity will then initiate the next cycle of uptake. Auxin can obviously interact with this process and thus maintain actin dynamicity in the presence of BP100. This is supported by the observation that the actin elongation rate, which is strongly reduced after treatment with BP100, is rescued by exogenous IAA (**Supplementary Table S1**). The preferential uptake of BP100 into the terminal cells of a file (**Fig. 2**) might be linked with the fact that these cells act as sources for endogenous auxin and are also endowed with a higher abundance of the actin-nucleation factor actin-related protein 3 (Maisch et al. 2009). As expected, this apical dominance of BP100 uptake is sensitive to manipulation of auxin status, for instance by inhibitors of auxin transport or by adding excess exogenous auxin.

Superoxide as missing link?

BP100 per se is not binding to actin (Eggenberger et al. 2011), which means that the bundling of actin filaments must be mediated indirectly, by a transducing event that is triggered when BP100 binds to the membrane. The mechanisms underlying this transduction event are not known, but one can deduce two criteria: (i) the transducing molecules must cross the cell membrane and then interact with actin-associated proteins at the inner face of the cell membrane; and (ii) the transducing molecules must be responsive to auxin. Both criteria are met by superoxide anions that are generated by the apoplastic oxidative burst and penetrate through the cell membrane into the cell interior. We propose that BP100 interacts with a second circuit that involves superoxide anions generated by the NADPH oxidase RbohH, and actin (**Fig. 6**, red numbers). Glutathionylation of actin caused by superoxide (Dixon et al. 2005) sequesters G-actin from incorporation into actin filaments (Lassing et al. 2007). As a result, dynamic actin filaments will be eliminated due to their innate turnover, whereas stable actin cables will accumulate. This might be one of the molecular mechanisms underlying the observed decrease in the rate of filament elongation and shortening (**Supplementary Table S1**). At the same time, the superoxide anions will activate the G-protein Rac (Moldovan et al. 1998) which in turn activates phospholipase D, as important signaling hub, already mentioned above (Wu et al. 2011). One of its products, PA, not only sequesters actin-capping proteins (allowing for elongation of actin filaments and concomitant decrease of actin cables), but can also recruit Rac to activate RbohH itself (Wong et al. 2007). This diversion of Rac will not only constitute a self-amplification of RbohH activity, but will also further suppress actin elongation and thus stimulate bundling.

This RbohH–actin oscillator is now linked with the auxin–actin oscillator by superoxide as the common signal (**Fig. 6**), since the activation of Rac by auxin has been shown to be conveyed by superoxide (Wu et al. 2011). The biological function of this link between the two oscillators might be needed to partition resources between growth (induced by auxin) and stress resilience (induced by RbohH).

To dissect the interaction between these oscillators, we used DPI as a tool. This inhibitor of NADPH-dependent flavoproteins inhibits at low concentrations, supporting its specificity. However, a potential second target of this inhibitor might be membrane-bound nitric oxide synthases (NOSs) that are NADPH-dependent flavoproteins as well and have been shown in mammalian cells to be inhibited by DPI (Stuehr et al. 1991). Albeit that a membrane-located putative NOS activity has been published for tobacco roots (Stöhr et al. 2001), so far, despite intensive search, no molecular homolog of the mammalian NADPH-dependent NOS could be identified in plants. Instead, NO in plant cells is derived from the cytosolic nitrate reductase (Mur et al. 2013). The absence of plant NOS as a second target for DPI, as well as the very low concentration of DPI required to obtain a cellular response (200 nM) emphasize the specificity of this inhibitor. We therefore used DPI to address the role of RbohH-dependent oxidative burst for the bundling of actin in response to BP100, and found that DPI could restore actin dynamicity in a manner similar to auxin (**Fig. 5**; **Supplementary Movies S5–S7**). In previous work, we had already shown in grapevine cells that actin bundling induced by the bacterial elicitor Harpin, which induces RbohH, can be mitigated by pre-treatment with auxin. Moreover, the auxin effect can be mimicked by *n*-butanol, a specific inhibitor of phospholipase D, but not by the inactive analog *sec*-butanol (Chang et al. 2015). In both cases, superoxide generated by RbohH has been found to be necessary for the bundling response of actin, and in both cases the apoplastic oxidative burst is induced by a perturbation of membrane integrity—either by the pore-forming Harpin protein or by the membrane passage of BP100. It should be mentioned here that DPI alone caused a heterogenous response—while actin dynamicity persisted in some cells (**Fig. 5D**), it was decreased in others. This heterogeneity might depend on the levels of superoxide accumulated in the cell wall prior to addition of the inhibitor. It remains to be

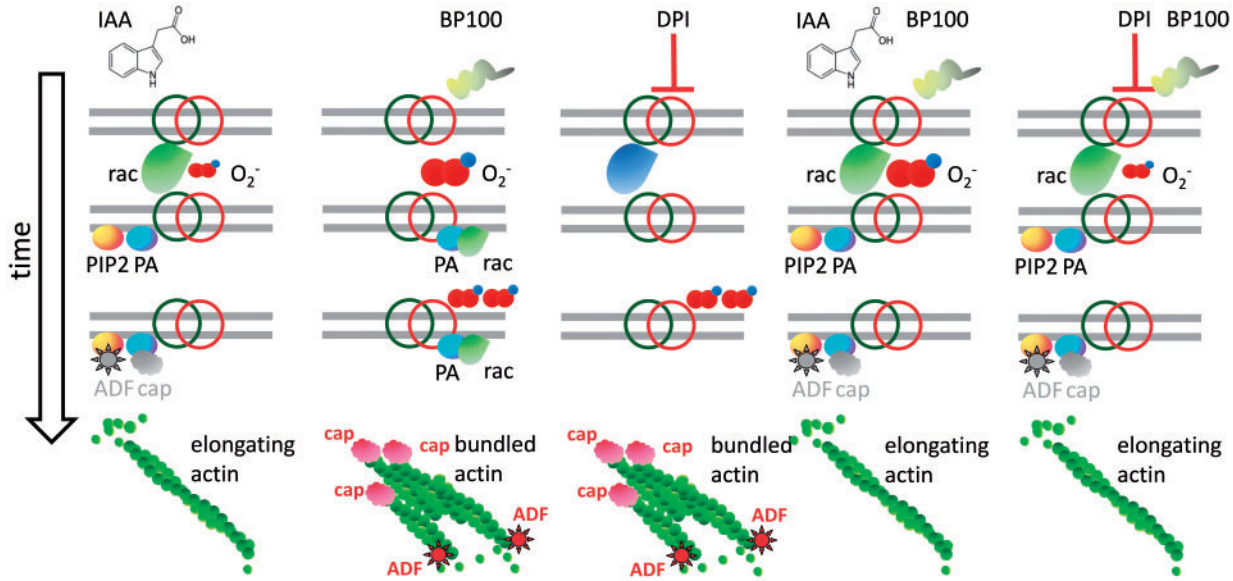

Fig. 7 Implications derived from the working model depicted in **Fig. 6** for the experimental conditions used in this study. Green circles represent the auxin–actin circuit, red circles represent the RboH–actin circuit. PA, phosphatidic acid; PIP_2, phosphatidyl inositol-4,5-bisphosphate; ADF, actin-depolymerization factor; cap, capping protein, DPI, diphenylene iodonium; IAA, natural auxin. Inactive Rac is depicted in blue, active Rac in green; ADF and cap in gray represent the inactive forms sequestered to the membrane.

elucidated to what extent pools of superoxide in the apoplast differ depending on the progression into cell expansion.

Conclusions and outlook

Our working model (**Fig. 6**) should not be seen as a static structure, but rather as a dynamic process: the response of actin filaments to BP100 is linked with regulatory circuits across the cell membrane that either are acting in the context of hormonal signaling (auxin–actin oscillator) or are involved in the sensing of membrane integrity (RboH–actin oscillator). Both circuits converge at superoxide (acting in concert with the small GTPase Rac1) as a transmembrane signal that is then read out by a signaling hub, involving phospholipase D and its products, mainly PA and PIP_2 that modulate actin remodeling by sequestering actin modifiers, such as actin-depolymerization factors and capping proteins. If used in a dynamic manner, this model can explain several non-intuitive features observed in the cellular response to BP100 (**Fig. 7**): the fact that both BP100 and, in a significant fraction of cells, DPI can cause actin bundling, if administered alone, while their combination will leave actin dynamicity intact is explained by mutual competition of two circuits for superoxide and the small GTPase Rac1. Furthermore, the self-amplification of the two circuits is predicted to lead to non-linear phase transitions in the response of actin. This implication of the model can explain the finding that uptake of BP100 is discontinuous, and that the rescue of actin dynamicity by DPI can also qualitatively differ even between neighboring cells within a cell file. This model further stimulates new questions which will be addressed in future research. (i) Can we find cell-penetrating-peptides that can evade 'detection' by the RboH–actin circuit in order to generate tools for chemical engineering that are as non-invasive as possible? (ii) Can we find other cell-penetrating peptides that, controlled by a simple external trigger, efficiently activate the RboH–actin circuit in order to induce programmed cell death in cells that have been invaded by biotrophic pathogens? (iii) By what mechanism can actin modulate the passage of BP100 into plant cells? (iv) Can we, by modulating the RboH–actin oscillator by appropriate auxin pre-treatment, improve the application of BP100 as a tool for chemical engineering? (5) Can we identify which member of the RboH family is involved in the oscillator (for instance by expression of dominant-negative versions)?

Materials and Methods

Peptide synthesis

BP100 was synthesized using standard 9-fluorenylmethoxycarbonyl (Fmoc) solid phase peptide synthesis protocols and labeled with FITC at the N-terminus as previously described (Eggenberger et al. 2011). The peptide was cleaved from the solid phase and purified by HPLC (Afonin et al. 2003, Wadhwani et al. 2006, Wadhwani et al. 2008), and characterized by analytical liquid chromatography combined with mass spectrometry (LC-MS).

Cell lines

The tobacco cell line BY-2 (*Nicotiana tabacum* L. cv. Bright Yellow 2) was cultivated in liquid medium containing Murashige and Skoog salts (4.3 g l^{-1}) (Duchefa), sucrose (30 g l^{-1}), KH_2PO_4 (200 mg l^{-1}), inositol (100 mg l^{-1}), thiamine (1 mg l^{-1}) and 2,4-D (0.2 mg l^{-1}) at pH 5.8 (Nagata et al. 1990). Cells were subcultured weekly, inoculating 1–1.5 ml of stationary cells into 30 ml of fresh medium in 100 ml Erlenmeyer flasks. The cell suspensions were incubated at 25 °C in the dark on an orbital shaker (KS250 basic, IKA Labortechnik) at 150 r.p.m. Stock BY-2 calli were maintained on media solidified with agar [0.8% (w/v)] and subcultured monthly. The transgenic cell line GF11 expressing the actin-binding domain of plant fimbrin was maintained on the same

medium supplemented with hygromycin (30 mg l^{-1}) (Sano et al. 2005). If not stated otherwise, the experiments were performed at 3 d after subcultivation.

Treatments and determination of viability and the mitotic index

For the evaluation of peptide toxicity, 50 µl of a 3-day-old cell suspension and 950 µl of culture medium were mixed in a 1.5 ml reaction tube. BP100 was then added to the cells to specified final concentrations between 1 and 10 µM and incubated for 24 h under continuous shaking. The concentrations were adjusted to the time of treatment based on the scope of the respective experiment—to test the cellular responses, a concentration of 1 µM BP100 was used, to measure short-term uptake of fluorescent BP100, higher concentrations (2–4 µM) were used to obtain a sufficient signal to noise ratio for reliable quantification. Control experiments were performed in parallel, where the cells were treated in the same manner, but omitting the addition of CPPs. In some experiments, cells were treated with DPI (Sigma-Aldrich), diluted from a 10 mM stock in dimethylsulfoxide (DMSO). These treatments were accompanied by solvent controls, where the maximal concentration of solvent used in the test samples was administered and did not exceed 0.1%. Following incubation, the cells were transferred to custom-made staining chambers (Nick et al. 2000) then thoroughly rinsed with 15 ml of fresh sterile culture medium. For inhibitor experiments, cells were pre-treated for 30 min with the inhibitor, before adding FITC-conjugated BP100. The mitotic index was quantified as described in Kühn et al. (2013). Viability was determined either by fluorescein diacetate (Widholm 1972) or by the Evan's Blue dye exclusion test (Gaff and Okong'O-Ogola 1971) based on at least 750 cells per data point.

Determination of BP100 uptake

If not stated otherwise, 2 µM FITC-conjugated BP100 was used to quantify uptake by means of the Image J software (http://rsb.info.nih.gov/ij/). To ensure comparability, all images were acquired under standardized conditions (exposure time, brightness, contrast and gamma corrections) inactivating the automatic optimization protocol of the Axiovision system used for imaging. Fluorescence intensity was averaged over the interior of the cell using the freehand selection tool of the software and corrected for background against a reference area outside of the target cell.

Long-term observation of actin dynamics

For long-term observation of actin dynamics, 50 µl of stationary phase GF11 cell suspension were diluted with 950 µl of sterile culture medium and viewed immediately. Time lapses were recorded by taking a picture of a cross-section through the cells' cortical region every 30 s for up to 2 h. To assess the effect of BP100 on actin dynamics it was added at a final concentration of 1 µM and evaluated directly or after incubation for 2 h under continuous shaking. Time lapses were recorded for each experimental set-up as described above. As addition of BP100 to the cells resulted in an increased actin rigidity, control experiments were performed in order to find out whether addition of the plant hormone and actin-debundling agent auxin (Maisch and Nick 2007) would be able to reverse the rigid actin phenotype. Therefore, 2 µM auxin was added to the cells at the same time as BP100 or after incubation with the CPP for 2 h.

Microscopic analysis

The samples were examined under an AxioImager Z.1 microscope (Zeiss) equipped with an ApoTome microscope slider for optical sectioning and a cooled digital CCD camera (AxioCamMRm). For the observation of GFP fluorescence, filter set 38 HE was used (excitation at 470 nm, beamsplitter at 495 nm and emission at 525 nm) (Zeiss). The DNA signal was recorded through filter set 49 (excitation at 365 nm, beamsplitter at 395 nm and emission at 445 nm) (Zeiss). Images, as well as time-lapse recordings, were analyzed using the Axio-Vision (release 4.5) software and processed for publication using Photoshop (release 5.5, Adobe Systems).

Quantification of actin responses

To obtain a global measure for the dynamic change, actin dynamicity was assessed using the Image J software (National Institute of Health). Frames from the time series were inverted and thresholded into binary images to exclude the impact of fluorophore bleaching. The differential of a region of interest between subsequent frames:

$$\int |p(t+1) - -p(t)|$$

$\int |p(t+1) - p(t)$ with $p(t+1)$ and $p(t)$ the intensity value for a given pixel at time point t or $t+1$, respectively (the possible values were either 0 or 255, due to the thresholding) was then divided by the area of the scored region of interest. Upon active remodeling, this value was high, whereas in a situation of 'actin freezing', this value was low (**Fig. 3D**). Dynamicity was a global measure comprising different processes, such as actin elongation, actin shrinkage/severing, or lateral displacement of actin filaments (swaying), as exemplarily indicated in **Fig. 3E**. To relate actin dynamicity to these processes, individual actin filaments were randomly selected and followed over subsequent frames to extract changes of length over time using the perimeter tool of Image J. These values were subjected to a linear regression to extract the parameters of elongation and shortening (**Supplementary Table S1**). We did not discriminate between continuous shortening and discontinuous shortening (for instance, caused by severing). To quantify apparent bundle thickness, grids of equally spaced probing lines of 8 pixel width were layered over the cell, four aligned with the long and four aligned with the short axis, and intensity profiles were collected along these lines using the density profile tool. The line width of 8 pixels is important to filter out random fluctuations and to improve the robustness of the profile. For each position along this profile d_i, the first derivative d_i' was divided by d_i, yielding a value of + 1 in the rising flank of an actin bundle, and a value of −1 in the dropping flank, whereas the value will be 0 in the trough between two filaments. Random fluctuations of fluorescence intensity in the trough were filtered out by multiplication with the preceding value in the profile. (which was most probably 0). By squaring all values, all pixels that that were part of F-actin obtain a value of 1. The sum over the profile S thus yields the fraction of the profile covered by actin. To determine the number of filaments along this profile, each value was subtracted from the preceding value. At the leading edge of a filament, this value will be −1, at the trailing edge of a filament, this value will be + 1, and it will be 0 in the trough between filaments or in the interior of the filament. By summing up the squares of these numbers and dividing this value by 2 (because each filament has a leading and a trailing edge contributing to the value), the number of actin filaments across the profile can be determined. The average width of F-actin, w, can now be derived as ratio of S and the number of filaments. The values obtained for the eight profiles across a cell are averaged.

Supplementary data

Supplementary data are available at PCP online.

Funding

This work was supported by the Center for Functional Nanostructures (CFN) [TP E1.2 and E1.3]; the German Research Council (DFG) [a cluster of excellence].

Acknowledgments

The technical support of S. Purper in the cultivation of the cell lines is gratefully acknowledged.

Disclosures

The authors have no conflicts of interest to declare.

References

Afonin, S., Glaser, R.W., Berditchevskaja, M., Wadhwani, P., Gührs, K.H., Möllmann, U., et al. (2003) 4-Fluoro-phenylglycine as a label for ^{19}F-NMR structure analysis of membrane-associated peptides. *Chembiochem* 4: 1151–1163.

Badosa, E., Ferre, R., Francés, J., Bardají, E., Feliu, L., Planas, M., et al. (2009) Sporicidal activity of synthetic antifungal undecapeptides and control of Penicillium rot of apples. *Appl. Environ. Microbiol*. 75: 5563–5569.

Badosa, E., Ferre, R., Planas, M., Feliu, L., Besalú, E., Cabrefiga, J., et al. (2007) A library of linear undecapeptides with bactericidal activity against phytopathogenic bacteria. *Peptides* 28: 2276–2285.

Boevink, P., Oparka, K., Santa Cruz, S., Martin, B., Betteridge, A. and Hawes, C. (2002) Stacks on tracks: the plant Golgi apparatus traffics on an actin/ER network. *Plant J.* 15: 441–447.

Chang, M., Chou, J.C. and Lee, H.J. (2005) Cellular internalization of fluorescent proteins via arginine-rich intracellular delivery peptide in plant cells. *Plant Cell Physiol*. 46: 482–488.

Chang, X., Riemann, M. and Nick, P. (2015) Actin as deathly switch? How auxin can suppress cell-death related defence. *PLoS One* 10: e0125498.

Chugh, A. and Eudes, F. (2007) Translocation and nuclear accumulation of monomer and dimer of HIV-1 Tat basic domain in triticale mesophyll protoplasts. *Biochim. Biophys. Acta* 1768: 419–426.

Chugh, A. and Eudes, F. (2008) Cellular uptake of cell-penetrating peptides pVEC and transportan in plants. *J. Peptide Sci.* 14: 477–481.

Colombo, M., Mizzotti, C., Masiero, S., Kater, M.M. and Pesaresi, P. (2015) Peptide aptamers: the versatile role of specific protein function inhibitors in plant biotechnology. *J. Integr. Plant Biol.* 57: 892–901.

Deeks, MJ, Fendrych, M, Smertenko, A, Bell, KS, Oparka, K and Cvrckova, F, et al. (2010) The plant forming AtFH4 interacts with both actin and microtubules, and contains a newly identified microtubule-binding domain. *J Cell Sci*. 123: 1209–1215.

Dixon, D.P., Skipsey, M., Grundy, N.M. and Edwards, R. (2005) Stress-induced protein S-glutathionylation in Arabidopsis. *Plant Physiol.* 138: 2233–2244.

Durst, S., Nick, P. and Maisch, J. (2013) Actin-depolymerizing factor 2 is involved in auxin dependent patterning. *J. Plant Physiol.* 170: 1057–1066.

Eggenberger, K., Mink, C., Wadhwani, P., Ulrich, A.S. and Nick, P. (2011) Using the peptide BP100 as a cell penetrating tool for chemical engineering of actin filaments within living plant cells. *Chembiochem* 12: 132–137.

Eggenberger, K., Schröder, T., Birtalan, E., Bräse, S. and Nick, P. (2009) Passage of Trojan peptoids into plant cells. *Chembiochem* 10: 2504–2512.

Fanghänel, S., Wadhwani, P., Strandberg, E., Verdurmen, W.P.R., Bürck, J., Ehni, S., et al. (2014) Structure analysis and conformational transitions of the cell penetrating peptide transportan 10 in the membrane-bound state. *PLoS One* 9: e99653.

Ferre, R., Badosa, E., Feliu, L., Planas, M., Montesinos, E. and Bardají, E. (2006) Inhibition of plant pathogenic bacteria by short synthetic cecropinA–melittin hybrid peptides. *Appl. Environ. Microbiol.* 72: 3302–3308.

Gaff, D.F. and Okong'O-Ogola (1971) The use of non-permeating pigments for testing the survival of cells. *J. Exp. Bot.* 22: 756–758.

Gao, N., Wadhwani, P., Mühlhäuser, P., Liu, Q., Riemann, M., Ulrich, A., et al. (2016) An antifungal protein from *Ginkgo biloba* binds actin and can trigger cell death. *Protoplasma* 253: 1159–1174.

Guan, X., Buchholz, G. and Nick, P. (2014) Actin marker lines in grapevine reveal a gatekeeper function of guard cells. *J. Plant Physiol*. 171: 1164–1173.

Hohenberger, P., Eing, C., Straessner, R., Durst, S., Frey, W. and Nick, P. (2011) Plant actin controls membrane permeability. *Biochim. Biophys. Acta* 1808: 2304–2312.

Jiang, R.H.Y. and Tyler, B.M. (2012) Mechanisms and evolution of virulence in oomycetes. *Annu. Rev. Phytopathol.* 50: 295–318.

Kadota, A., Yamada, N., Suetsugu, N., Hirose, M., Saito, S. and Shoda, K. (2009) Short actin-based mechanism for light-directed chloroplast movement in Arabidopsis. *Proc. Natl. Acad. Sci. USA* 106: 13106–13111.

Kühn, S., Liu, Q., Eing, C., Wüstner, R. and Nick, P. (2013) Nanosecond electric pulses target to a plant-specific kinesin at the plasma membrane. *J. Membr. Biol.* 246: 927–938.

Kusaka, N, Maisch, J, Nick, P, Hayashi, KI and Nozaki, H. (2009) Manipulation of Intercellular Auxin in a Single Cell by Light with Esterase-Resistant Caged Auxins. *ChemBioChem*. 10: 2195–2202.

Lassing, I., Schmitzberger, F., Bjornstedt, M., Holmgren, A., Nordlund, P. and Schutt, C.E. (2007) Molecular and structural basis for redox regulation of beta-actin. *J. Mol. Biol.* 370: 331–348.

Li, J.J., Henty-Ridilla, J.L., Huang, S.H., Wang, X., Blanchoin, L. and Staiger, C.J. (2012) Capping protein modulates the dynamic behavior of actin filaments in response to phosphatidic acid in Arabidopsis. *Plant Cell* 24: 3742–3754.

Liu, Q., Qiao, F., Ismail, A., Chang, X. and Nick, P. (2013) The plant cytoskeleton controls regulatory volume increase. *Biochim. Biophys. Acta* 1828: 2111–2120.

Maisch, J., Fišerová, J., Fischer, L. and Nick, P. (2009) Actin-related protein 3 labels actin-nucleating sites in tobacco BY-2 cells. *J. Exp. Bot.* 60: 603–614.

Maisch, J. and Nick, P. (2007) Actin is involved in auxin-dependent patterning. *Plant Physiol*. 143: 1695–1704.

Mathur, J., Mathur, N. and Hülskamp, M. (2002) Simultaneous visualization of peroxisomes and cytoskeletal elements reveals actin and not microtubule-based peroxisome motility in plants. *Plant Physiol.* 128: 1031–1045.

Mizuno, T., Miyashita, M. and Miyagawa, H. (2009) Cellular internalization of arginine rich peptides into tobacco suspension cells: a structure–activity relationship study. *J. Peptide Sci*. 15: 259–263

Moldovan, L., Irani, K., Moldovan, N.I., Finkel, T. and Goldschmidt-Clermont, P.J. (1998) The actin cytoskeleton reorganization induced by Rac1 requires the production of superoxide. *Antioxid. Redox Signal*. 1: 29–43.

Mur, LA1, Mandon, J, Persijn, S, Cristescu, SM, Moshkov, IE, Novikova, GV, Hall, MA, Harren, FJ, Hebelstrup, KH and Gupta, KJ. (2013) Nitric oxide in plants: an assessment of the current state of knowledge. *AoB Plants*. doi: 10.1093/aobpla/pls052. Epub 2013 Jan 31.

Nagata, T., Nemoto, Y. and Hasezawa, S. (1992) Tobacco BY-2 cell line as the 'Hela' cell in the cell biology of higher plants. *Int. Rev. Cytol*. 132: 1–30.

Nick, P. (2010) Probing the actin–auxin oscillator. *Plant Signal. Behav.* 5: 4–9.

Nick, P., Han, M. and An, G. (2009) Auxin stimulates its own transport by actin reorganization. *Plant Physiol.* 151: 155–167.

Nick, P., Heuing, A. and Ehmann, B. (2000) Plant chaperonins: a role in microtubule-dependent wall-formation? *Protoplasma* 211: 234–244.

Opatrný, Z., Nick, P. and Petrášek, J. (2014) plant cell strains in fundamental research and applications. In Applied Plant Cell Biology. Plant Cell Monographs, Vol. 22. Edited by Nick, P. and Opatrný, Z. pp. 455–481. Springer, Berlin

Qiao, F., Petrášek, J. and Nick, P. (2010) Light can rescue auxin-dependent synchrony of cell division. *J. Exp. Bot.* 61: 503–510.

Ressad, F., Didry, D., Xia, G.X., Hong, Y., Chua, N.H., Pantaloni, D., et al. (1998) Kinetic analysis of the interaction of actin-depolymerizing factor (ADF)/cofilin with G- and F-actins: comparison of plant and human ADFs and effect of phosphorylation. *J. Biol. Chem*. 273: 20894–20902.

Sano, T., Higaki, T., Oda, Y., Hayashi, T. and Hasezawa, S. (2005) Appearance of actin microfilament 'twin peaks' in mitosis and their function in cell plate formation, as visualized in tobacco BY-2 cells expressing GFP–fimbrin. *Plant J.* 44, 595–605.

Sheahan, M.B., Rose, R.J. and McCurdy, D.W. (2007) Actin-filament-dependent remodeling of the vacuole in cultured mesophyll protoplasts. *Protoplasma* 230: 141–152.

Stöhr, C., Strube, F., Marx, G., Ullrich, W.R. and Rockel, P. (2001) A plasma membrane-bound enzyme of tobacco roots catalyses the formation of nitric oxide from nitrite. *Planta* 212: 835–841.

Smertenko, AP, Deeks, MJ and Hussey, PJ (2010) Strategies of actin reorganisation in plant cells. *J Cell Sci*. 123: 3019–3028.

Stuehr, D.J., Fasehun, O.A., Kwon, N.S., Gross, S.S., Gonzalez, J.A., Levi, R., et al. (1991) Inhibition of macrophage and endothelial cell nitric oxide synthase by diphenyleneiodonium and its analogs. *FASEB J.* 5: 98–103.

Su, H., Wang, T., Dong, H.J. and Ren, H.Y. (2007) The Villin/Gelsolin/Fragmin superfamily proteins in plants. *J. Integr. Plant Biol.* 49: 1183–1191.

Thomas, C., Hoffmann, C., Dieterle, M., Van Troys, M., Ampe, C. and Steinmetz, A. (2006) Tobacco WLIM1 is a novel F-actin binding protein involved in actin cytoskeleton remodeling. *Plant Cell* 18: 2194–2206.

Unnamalai, N., Kang, B.G. and Lee, W.S. (2004) Cationic oligopeptide-mediated delivery of dsRNA for post-transcriptional gene silencing in plant cells. *FEBS Lett.* 566: 307–310.

Van Gestel, K., Kohler, R.H. and Verbelen, J.P. (2002) Plant mitochondria move on F-actin, but their positioning in the cortical cytoplasm depends on both F-actin and microtubules. *J. Exp. Bot.* 53: 659–667.

Van Troys, M., Huyck, L., Leyman, S., Dhaese, S., Vandekerkhove, J.I. and Ampe, C. (2008) Ins and outs of ADF/cofilin activity and regulation. *Eur. J. Cell Biol.* 87: 649–667.

Wadhwani, P., Afonin, S., Ieronimo, M., Buerck, J. and Ulrich, A.S. (2006) Optimized protocol for synthesis of cyclic gramicidin S: starting amino acid is key to high yield. *J. Org. Chem.* 71: 55–61.

Wadhwani, P., Buerck, J., Strandberg, E., Mink, C., Afonin, S., Ieronimo, M., et al. (2008) Using a sterically restrictive amino acid as a 19F-NMR label to monitor and to control peptide aggregation in membranes. *J. Amer. Chem. Soc.* 130: 16515–16517

Wender, P.A., Mitchell, D.J., Pattabiraman, K., Pelkey, E.T., Steinman, L. and Rothbard, J.B. (2000) The design, synthesis, and evaluation of molecules that enable or enhance cellular uptake: peptoid molecular transporters. *Proc. Natl. Acad. Sci. USA* 97: 13003–13008.

Widholm, J.M. (1972) The use of fluorescein diacetate and phenosafranine for determining viability of cultured plant cells. *Stain Technol.* 47: 189–194.

Wong, H.L., Pinontoan, R., Hayashi, K., Tabata, R., Yaeno, T. and Hasegawa, K. (2007) Regulation of rice NADPH oxidase by binding of RacGTPase to its N-terminal extension. *Plant Cell* 19: 4022–4034.

Wu, H.M., Hazak, O., Cheung, A.Y. and Yalovsky, S. (2011) RAC/ROP GTPases and auxin signaling. *Plant Cell* 23: 1208–1218.

Zaban, B., Maisch, J. and Nick, P. (2013) Dynamic actin controls polarity induction de novo in protoplasts, *J. Int. Plant Biol.* 55: 142–159.

Zhu, J. and Geisler, M. (2015) Keeping it all together: auxin–actin crosstalk in plant development. *J. Exp. Bot.* 66: 4983–4998.